Radiation Measurements 191 (2026) 107592

Contents lists available at ScienceDirect

Radiation Measurements

journal homepage: www.elsevier.com/locate/radmeas

A novel wearable dosimeter system that can analyze the incident direction of X-rays for medical dosimetry – Improvements to the detector arrangements and analysis algorithm –

Takashi Asahara [a], Rina Nishigami [b], Daiki Kobayashi [b], Natsumi Kimoto [c], Sota Goto [d], Kazuki Takegami [e], Rin Ishii [f], Mana Mitani [g], Mitsugi Honda [g], Toshihiro Iguchi [a], Hiroaki Hayashi [f,*]

[a] Department of Radiological Technology, Faculty of Health Sciences, Okayama University, 2-5-1 Shikata-cho, Kita-Ku, Okayama, Okayama, 700-8558, Japan
[b] Graduate School of Medical Sciences, Kanazawa University, 5-11-80 Kodatsuno, Kanazawa, Ishikawa, 920-0942, Japan
[c] Department of Radiological Science, Faculty of Health Sciences, Junshin Gakuen University, 1-1-1 Chikushigaoka, Minami-Ku, Fukuoka, Fukuoka, 815-8510, Japan
[d] Faculty of Health Science, Kobe Tokiwa University, 2-6-2 Otani, Nagata-Ku, Kobe, Hyogo, 653-0838, Japan
[e] Department of Radiological Technology, Yamaguchi University Hospital, 1-1-1 Minamikogushi, Ube, Yamaguchi, 755-8505, Japan
[f] College of Transdisciplinary Sciences for Innovation, Kanazawa University, Kakuma-machi, Kanazawa, Ishikawa, 920-1192, Japan
[g] Division of Radiological Technology, Medical Support Department, Okayama University Hospital, 2-5-1 Shikata-cho, Kita-Ku, Okayama, Okayama, 700-8558, Japan

ARTICLE INFO

Keywords:
Wearable active-type dosimeter
X-ray incident direction
Occupational dose
Interventional radiology

ABSTRACT

When performing real-time dosimetry using an active-type dosimeter during clinical fluoroscopic procedures, angular dependence of dosimeter response should be taken into account. Our research group addressed this issue and proposed a triple-type dosimeter that can determine the incident angle of scattered X-rays. The triple-type detector consists of three active dosimeters. The two side dosimeters have slope filters to enhance the angular dependence and are intentionally tilted. The central dosimeter faces forward. The incident angle of X-rays (θ_{in}) is estimated using the signal differences between the central dosimeter and the left and/or right dosimeters. Then, the absolute dose is determined by correcting the angular dependence of the central dosimeter based on the estimated θ_{in}. In order to verify the concept of the triple-type dosimeter, we conducted a proof-of-concept experiment using clinical X-ray fluoroscopic equipment. Scattered X-rays were generated by irradiating an elliptical cylindrical water phantom. The response of the triple-type dosimeter was evaluated by rotating it to vary the incident angle of scattered X-rays generated by the water phantom. The proposed dosimetry system could estimate the θ_{in} over an angular range of ±80° (with uncertainty of 1.35°), which is 30° wider than the previous version, and successfully determined the absolute doses after correction for the angular dependence of the dosimeter. Although the active-type dosimeter had a systematic uncertainty related to the angular dependence of ±15.2 %, our system succeeded in reducing the systematic uncertainty to ±3.2 %.

1. Introduction

When measuring radiation dose in clinical settings, it is very important to consider the angular dependence of the dosimeter response. This is because the diagnostic X-rays used in medicine are relatively lower energy, and the structural asymmetry of the detectors results in large angular dependence [Dong et al., 2011; Silva et al., 2016; Goto et al., 2020]. Passive dosimeters such as optically stimulated luminescence dosimeter (OSL) have a relatively simple structure [Asahara et al., 2018, 2020; Jursinic, 2007], so attempts have been made to manufacture bioequivalent elements that have little dependence on angle and energy, and they have been applied to medical

This article is part of a special issue entitled: SSD21 published in Radiation Measurements.

* Corresponding author.
E-mail addresses: takashi.asahara.111@gmail.com (T. Asahara), nishigami.rina@gmail.com (R. Nishigami), kobayashi.daiki.2022@gmail.com (D. Kobayashi), natsumi.kimoto.0717@gmail.com (N. Kimoto), gotosota.19960221@gmail.com (S. Goto), kazuki-t@yamaguchi-u.ac.jp (K. Takegami), ishii.rin.0709@gmail.com (R. Ishii), m-mitani12@s.okayama-u.ac.jp (M. Mitani), honda-m@cc.okayama-u.ac.jp (M. Honda), iguchi@s.okayama-u.ac.jp (T. Iguchi), hayashi.hiroaki@staff.kanazawa-u.ac.jp (H. Hayashi).

https://doi.org/10.1016/j.radmeas.2025.107592
Received 31 July 2025; Received in revised form 21 November 2025; Accepted 12 December 2025
Available online 13 December 2025

dosimetry [Goto et al., 2023, 2025; Hayashi et al., 2021, 2025, 2026; Takegami et al., 2023; Maeda et al., 2026].

In contrast, active dosimeters are known to have relatively larger energy dependence because their detectors are fabricated with higher atomic-number materials. In addition, there are many restrictions on the dosimeter design related to the placement of the readout circuit, etc., making it extremely difficult to realize a detector that is not subject to angular dependence. Although basic data on the energy and angular dependences have been obtained and reported with the aim of furthering the clinical application of active dosimeters [Gangl et al., 2022; Hattori et al., 2023], no clinical research has been conducted in which proper corrections have been made based on these basic data. In other words, simply measuring the energy and angle dependences is not enough, and a more sophisticated detection systems need to be developed.

Active dosimeters can obtain real-time dose information. If the information on X-ray incident angle could be analyzed from the real-time data, this would not only enable analysis that eliminates angular dependence, but also make it possible to apply the incident X-ray angle data itself to dose reduction. Our research group previously developed a wearable "triple-type dosimeter" consisting of three active detectors [Asahara et al., 2023, 2024]. This dosimeter has two key functions: (1) analyzing the incident angle of X-rays, and (2) determining the absolute dose by correcting for angular dependence while simultaneously obtaining incident angle data. The previous version of the triple-type dosimeter had three active dosimeters arranged in a "line". The two side dosimeters had titanium slope filters to enlarge the angle dependence, and the X-ray incident angle was estimated from the signal difference between these two detectors. In the previous paper, a new function for analyzing the X-ray incident direction was successfully obtained, but the measurable angular view was limited to -50° to $+50^\circ$, which may not provide sufficient coverage for clinical use. When the signal from one of the left and right dosimeters became very small with a larger X-ray incident angle, the measurement uncertainty was increased. Moreover, while the previous studies employed a complex algorithm to analyze angles, the analyzed angles were in increments of 10°, leaving room for improvement.

The purpose of this research is to improve the performance of a triple-type dosimeter and develop the dosimeter that has a wider analytical view. To achieve this, a detector configuration arranged along a circular "arc" was devised. In addition, we modified the algorithm to analyze the X-ray incident angle using the signal difference between the central detector and a single side detector, rather than both side detectors. This updated procedure allows analysis of the X-ray incident direction based on measurement values with smaller uncertainties.

2. Materials and methods

2.1. A concept of a modified triple-type dosimeter system

In this section, the concept of the improved triple-type dosimeter is explained. Fig. 1 shows a conceptual illustration of the triple-type

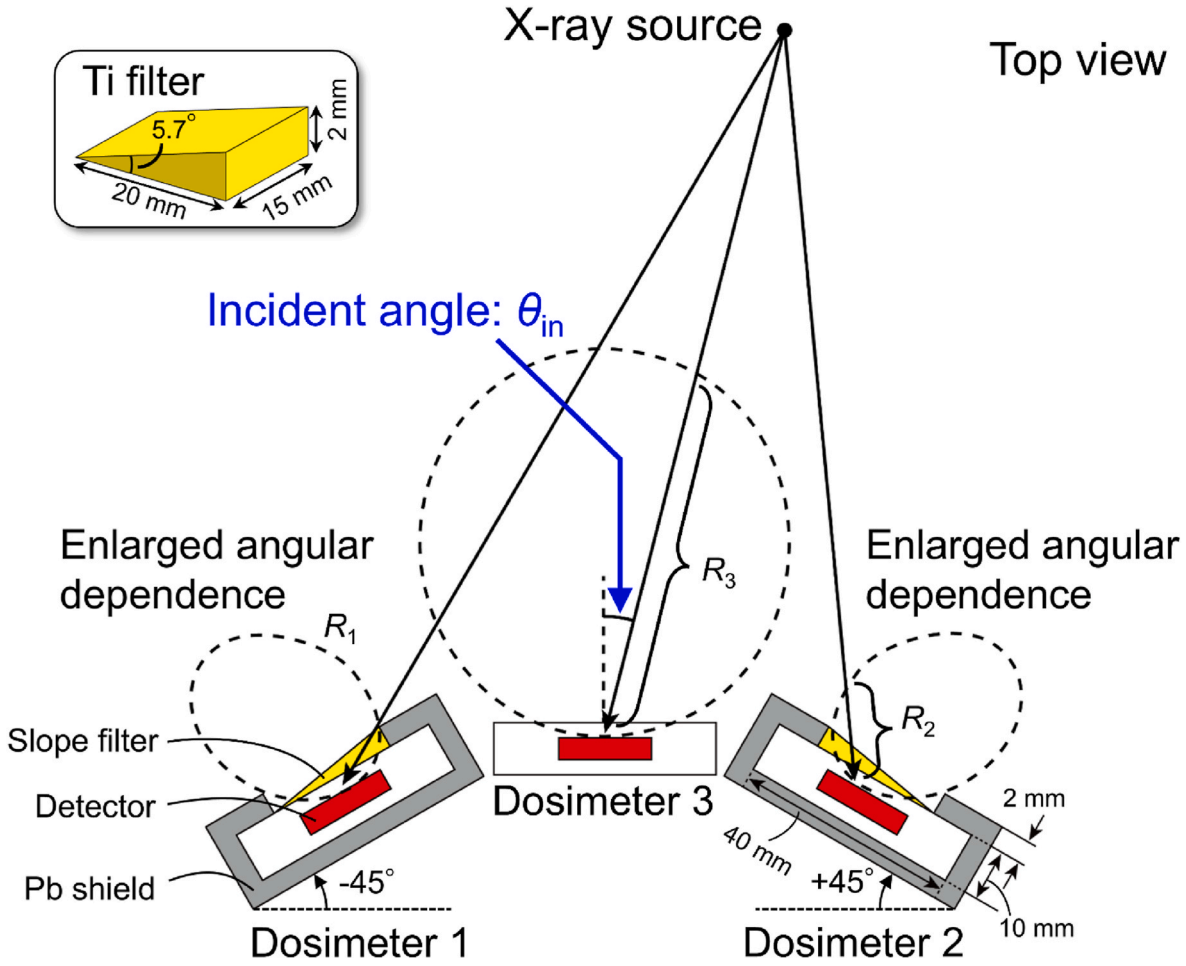

Fig. 1. Concept of the modified triple-type dosimeter system. The dashed ellipses show the angular dependence of the active-type dosimeters. Dosimeters 1 and 2 are arranged to have a titanium slope filter and lead shield to enlarge the angular dependence, and they are tilted $\pm 45^\circ$ outwards. The central dosimeter is a commercial dosimeter without modification. Based on the differences in measured responses R_1, R_2, and R_3, the incident angle of X-rays was derived.

dosimeter developed in this study. This dosimetry system consists of three active-type dosimeters. A major feature of our detection system is that the three dosimeters have different angular dependences. The dashed ellipses are the angular dependences of the dosimeters in polar coordinate form, where the frontal direction is defined as 0°. The X-ray incident angle was defined as θ_{in}.

Dosimeters 1 and 2 are RaySafe i2 dosimeters (Unfors RaySafe AB, Björklundabacken, Sweden) [Cardoso et al., 2016; Mangiarotti et al., 2016]. They are fixed at the left and right sides of a circular arc, and their inclination angles are set at ±45°. These dosimeters are shielded with 2 mm-thick lead in order to restrict the measurable X-rays to only those incident from the entrance window on the frontal surface. The back side is also shielded to reduce contamination from backscattering X-rays. To enlarge the angular dependence, the titanium slope filters are symmetrically arranged in front of the open windows. Therefore, the maximum thickness must be 2 mm to avoid protruding from the lead shield, and it has a linear slope from 0 mm to 2 mm (5.7°). The filter design has been determined by the previous study [Asahara et al., 2024], and this titanium filter has suitable performance in triple-type dosimeter. Dosimeter 1 has an angular view of approximately −50° to +50° [Asahara et al., 2023], and therefore, when tilted at −45°, it has a view of −95° to +5°. Dosimeter 2 was tilted +45°, resulting in a view of −5° to +95°. Dosimeter 3, the central dosimeter, is a RaySafe i3 (RaySafe i3; Unfors RaySafe AB, Björklundabacken, Sweden) [Cewe et al., 2022; Lundvall and Sandborg, 2022; Sanchez et al., 2021]; it has a reported sensitivity range of approximately ±90° and was used without modification [Unfors RaySafe, 2020]. For the experimental setup, an additional lead plate was placed on the back side of dosimeter 3, as with the other dosimeters, to reduce the influence of backscattering X-rays. Both the RaySafe i2 and i3 consist of silicon semiconductor detectors as their detection element.

As shown in Fig. 1, the responses of dosimeters 1, 2, and 3 are described as R_1, R_2, and R_3, respectively. When X-rays are incident from θ_{in}, the information of θ_{in} can be included in the signal difference between R_2 and R_3 (or R_1 and R_3), and therefore θ_{in} can be analyzed. Furthermore, by using this θ_{in} information with the angular dependence data determined in advance, it is possible to calculate the absolute dose by correcting the effect of θ_{in} on the measured dose as R_3. R_1, R_2, and R_3 are measured as the dose rate within a 1-s measurement period, which is personal dose equivalent at a 10 mm depth ($H_p(10)$) in units of mSv/h or μSv/s; this value is defined as the "response value" in this paper. These responses can be read in real-time using wireless communication technology and/or after the experiment using a dedicated communication device.

2.2. Analytical algorithm

Fig. 2 shows an analytical algorithm for deriving the incident angle θ_{in} and absolute dose using a triple-type dosimeter.

First, the θ_{in} is determined using the R_1, R_2, and R_3. R_3 derives from a centrally placed dosimeter that, unlike the other two dosimeters, is not subject to signal attenuation from an added Ti filter, so for most measurement data R_3 is larger than R_1 or R_2. The ratio of R_1 and R_2 to R_3 were calculated in order to extract information on the relative differences between them, and used these values to calculate the θ_{in}. The response ratios were calculated as:

$$r_1 = \frac{R_1}{R_3}, \tag{1-1}$$

$$r_2 = \frac{R_2}{R_3}. \tag{1-2}$$

Because these response ratios have unique relationships with the θ_{in}, reference conversion tables $r_1^{ref}(\theta)$ and $r_2^{ref}(\theta)$, which are a function of θ, could be determined in advance. That is, when the r_1 and r_2 values can be measured experimentally, θ_{in} is determined as:

$$\theta_{in} = \left(r_1^{ref}\right)^{-1}(r_1), \tag{2-1}$$

$$\theta_{in} = \left(r_2^{ref}\right)^{-1}(r_2). \tag{2-2}$$

For the actual analysis, since the data from the direction of the X-ray incident side gives a larger r value, the larger values of r_1 and r_2 were used to calculate θ_{in}. This analysis algorithm is shown in the red box in Fig. 2 and summarized as:

$$R_1, R_2, R_3 \overset{\text{Selection}}{\rightarrow} \text{Max}(r_1, r_2) \overset{\text{Conversion}}{\rightarrow} \theta_{in}. \tag{3}$$

Next, the absolute dose D_{abs} is calculated from R_3 with the angular dependence correction. The correction factor k_θ is defined as:

$$k_\theta(\theta) = \frac{R_3^{ref}(\theta)}{R_3^{ref}(0°)}, \tag{4}$$

where $R_3^{ref}(\theta)$ is the reference response of dosimeter 3 at the incident angle θ, which should be determined in advance, and $R_3^{ref}(0°)$ is that at the frontal incidence angle (θ = 0°). Using the correction factor k_θ evaluated at the θ_{in} determined above, the absolute dose D_{abs} is calculated from R_3 as:

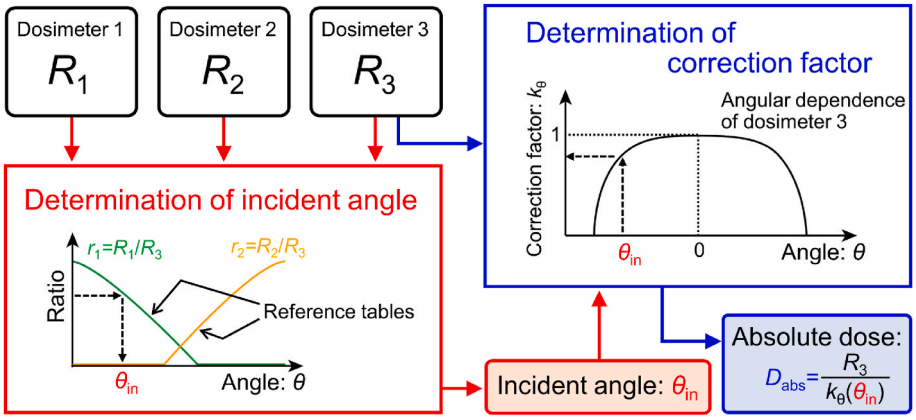

Fig. 2. An algorithm to determine both the incident angle θ_{in} and absolute dose D_{abs} using the triple-type dosimeter. The θ_{in} is determined using the response ratios R_1/R_3 and R_2/R_3. By using a reference conversion table that was determined in advance, the θ_{in} can be estimated from the response ratios. The D_{abs} is analyzed by correcting the angular dependence with the obtained θ_{in}.

$$D_{abs} = \frac{R_3}{k_\theta(\theta_{in})}. \quad (5)$$

This analysis algorithm is shown in the blue box in Fig. 2. Note that this correction does not aim to evaluate $H_p(10, \theta)$. Rather, the purpose of using k_θ is to correct for the angular dependence of the R_3 so that the D_{abs} represents the response at frontal incidence, i.e., an estimate equivalent to $H_p(10, 0^\circ)$. In other words, D_{abs} corresponds to the personal dose equivalent at 0° incidence, regardless of the incident angle.

By using this algorithm, the triple-type dosimeter system can determine both the incident angle θ_{in} and the absolute dose D_{abs}.

2.3. Experiment using the modified triple-type dosimeter

To verify the performance of the modified triple-type dosimeter, an experiment using a clinical fluoroscopic system was performed. Fig. 3 shows photographs of the experimental arrangement. A clinical X-ray fluoroscopic system (Ultimax-I, DREX-UI80; Canon Medical Systems, Tochigi, Japan) was used, with the X-ray tube set in the under-table configuration. The distance between the imaging detector and the X-ray focal point was set to 120 cm. An elliptical cylinder water phantom with outer dimensions of 30 cm × 45 cm × 20 cm^t [Japan Industrial Standard (JIS) Z4915, 1974] was placed on the table as a scatterer. The height of the center point at the phantom was set to 100 cm from the floor. The triple-type dosimeter was placed at the same height (100 cm from the floor). The irradiation field was 20 cm × 30 cm, and the horizontal distance between the dosimeter and the irradiation field was 50 cm. This arrangement simulated an operator with a dosimeter attached to the lower abdomen region. Although the proposed system is wearable dosimeter, they were mounted on a rotational actuator in this experiment to precisely control the incident angle. Because the back side of each dosimeter was shielded with lead, the measured scattered X-rays correspond to those entering only from the front surface, which is equivalent to the condition when worn on a human body. The irradiation conditions were 80 kV, 20 mA, 15 frames per second, and a pulse width of 10 ms. The automatic exposure control system was not used, allowing the dosimeter to be exposed to a higher dose. The scattered X-rays during the fluoroscopic procedure were measured. A rotational actuator (RCP2-RTBSL; IAI, Shizuoka, Japan) was used to precisely determine the rotation angle of the dosimeter from −120° to +120° at 10° intervals. The exposure time at each angle was 30 s.

Two measurements were performed. In both experiments, the response values were read after each irradiation and analyzed by the algorithm. The first irradiation was used to measure the response of the dosimeters. These data were then used to calibrate the reference tables ($r_1^{ref}(\theta)$ and $r_2^{ref}(\theta)$) and the correction factor (k_θ) for the angular dependence. To reduce statistical fluctuation, the average response values of 10-s measurements were used. The second irradiation was conducted to verify the feasibility of the triple-type dosimeter. The response values R_1, R_2, and R_3 observed every 1-s were analyzed. The incident angles analyzed using the algorithm were compared to the predetermined angles. Finally, the absolute dose with angular dependence correction, which is D_{abs} for 0° incidence, was determined using the incidence angle information, and the systematic uncertainty caused by the angular dependence was evaluated.

3. Results

3.1. Angular dependence

Fig. 4 shows the angular dependence of the triple-type dosimeter displayed on polar coordinates. Panels (a), (b), and (c) correspond to the responses from dosimeters 1, 2, and 3, respectively. The responses were obtained by rotating the dosimeter relative to the incident direction of the scattered X-rays, and these values are indicated as the integrated dose rate over a 10-s period in the unit of Sv. The coordinate system used in this experiment is shown in the inset; note that detectors 1 and 2 are tilted at −45° and +45°, respectively. Due to the slope filter and outward tilt arrangement, dosimeter 1 exhibited enhanced angular dependence, with increased sensitivity to X-rays incident from the left side (i.e., the negative angular direction). In turn, dosimeter 2, which was placed symmetrically on the opposite side, exhibited an enhanced angular dependence with increased sensitivity to X-rays incident from the positive angular direction. Strictly speaking, the distributions observed by detectors 1 and 2 were not symmetrical because the commercial RaySafe i2 detectors have asymmetric angular distributions [Cardoso et al., 2016; Mangiarotti et al., 2016]. The central dosimeter, dosimeter 3, which was not modified, showed very low angular dependence. However, the angular dependence was larger from directions exceeding ±45°, and therefore the effect of the angular dependence could not be ignored. The observed angular dependence was consistent with the manufacturer's reports [Unfors RaySafe, 2020]. The measured angular dependences indicate that the dosimeter's concept shown in Fig. 1 is feasible.

Fig. 5 (a) shows reference conversion tables $r_1^{ref}(\theta)$ and $r_2^{ref}(\theta)$, as a function of predetermined angle. The red and blue plots correspond to r_1

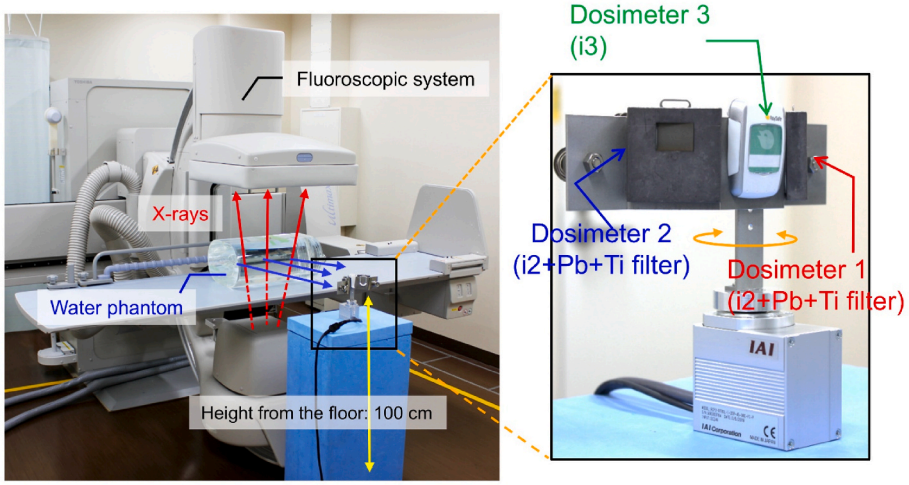

Fig. 3. Photograph of the experimental arrangement for performance verification of the triple-type dosimeter. The scattered X-rays from the water phantom were measured, and the dosimeter system was attached to the rotational actuator. The response values were observed when the angle was varied between −120° and +120° at 10° intervals.

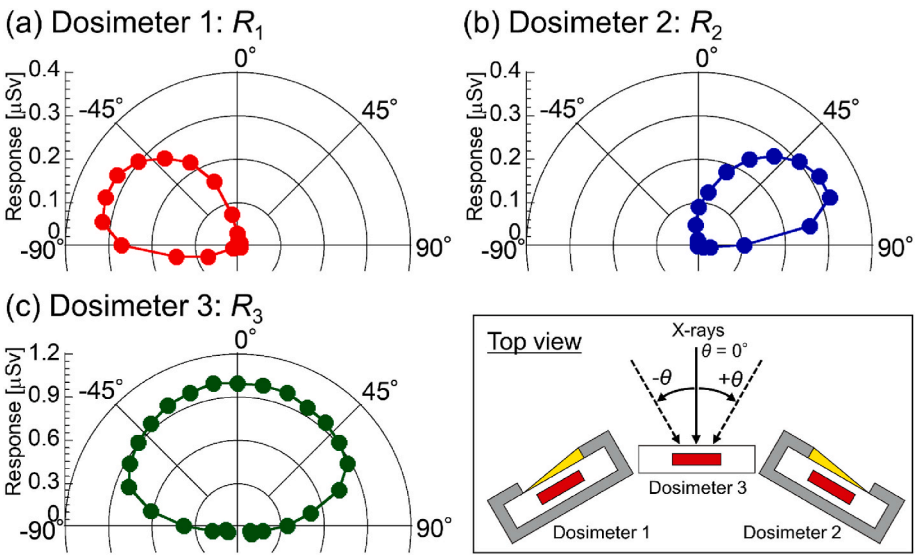

Fig. 4. Angular dependence of the modified triple-type dosimeter. (a) The response of dosimeter 1 shows an enlarged angular dependence for the negative angle side due to the tilted arrangement and slope filter. (b) The response of dosimeter 2 has the opposite sensitivity, which is enlarged for the positive direction. (c) The response of dosimeter 3 shows a relatively constant value within ±45°. The inset illustrates the top view of the dosimeter system, in which the angle is defined with respect to the central axis of the system.

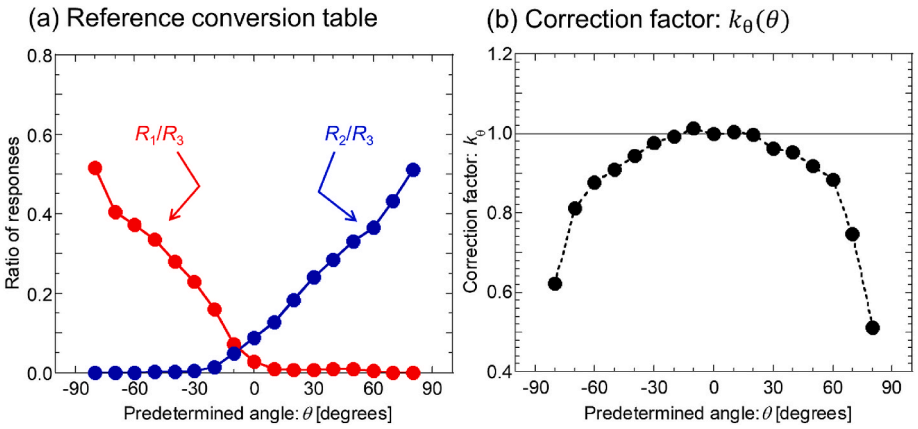

Fig. 5. Reference data used for the algorithm. Panel (a) shows the reference conversion tables of $r_1^{\mathrm{ref}}(\theta)$ and $r_2^{\mathrm{ref}}(\theta)$ for converting the response ratios as a function of the incident angle. Using them, the X-ray incident angle can be derived. Panel (b) shows the correction factor k_θ, which was calculated from the angular dependence of dosimeter 3. Using this data, the absolute dose can be calculated.

and r_2, respectively. A unique relationship can be seen within the range of −80° to +80°. The reference tables can be used to convert the measured response ratio to the incident angle. Fig. 5 (b) shows the correction factor k_θ, which is obtained from the measured response of dosimeter 3. Because it was shown that the correction factor is not a flat value, it must be corrected. Even when used within the narrow range of ±45°, a difference of approximately 10 % was observed. When the angle exceeds ±60°, the k_θ drops rapidly, down to approximately 0.5. Based on the k_θ and analyzed θ_{in}, our algorithm can calculate the absolute dose from the measured response.

3.2. Analysis of the incident angle and absolute dose

Fig. 6 shows the typical time-series measurement results of the incident angle θ_{in} and absolute dose D_{abs} analyzed by the modified triple-type dosimeter. For this demonstration, the predetermined angles were set to −70°, +60°, and 0°, and the dosimeter responses were recorded at 1-s intervals. Fig. 6 (a) shows the measured responses of each detector. Signals from detectors 1 and 3 were observed when the X-rays were incident from −70°. Signals from detectors 2 and 3 were observed when the X-rays were incident from +60°. When the X-rays were incident from 0°, signals from dosimeters 1, 2, and 3 were observed. Fig. 6 (b) shows the analyzed θ_{in} values. The mean angle and the standard deviation under the corresponding settings were determined as $-69.7 \pm 7.0°$, $58.1 \pm 3.6°$, and $0.2 \pm 3.3°$, which matched well with the predetermined θ_{in} values. Fig. 6 (c) shows the comparison between the original dose rate (without correction) and the D_{abs} rate calculated by our algorithm. D_{abs} values were constant regardless of θ_{in} values.

Fig. 7 (a) shows the results of the incident angle analyzed by our algorithm. They are the measurement results of 30-s average data taken from the time-series data (see Fig. 6). The horizontal and vertical axes are the predetermined and analyzed angles, respectively. Almost all data were plotted on the Y = X line. The standard deviation (SD) of residual uncertainty from the line was determined to be SD = 1.35°; this value was evaluated as the systematic uncertainty regarding the θ_{in} determination. Fig. 7 (b) compares the original dose rates and absolute dose rates obtained from dosimeter 3. By applying our correction procedure, the D_{abs} could be determined while eliminating systematic uncertainty

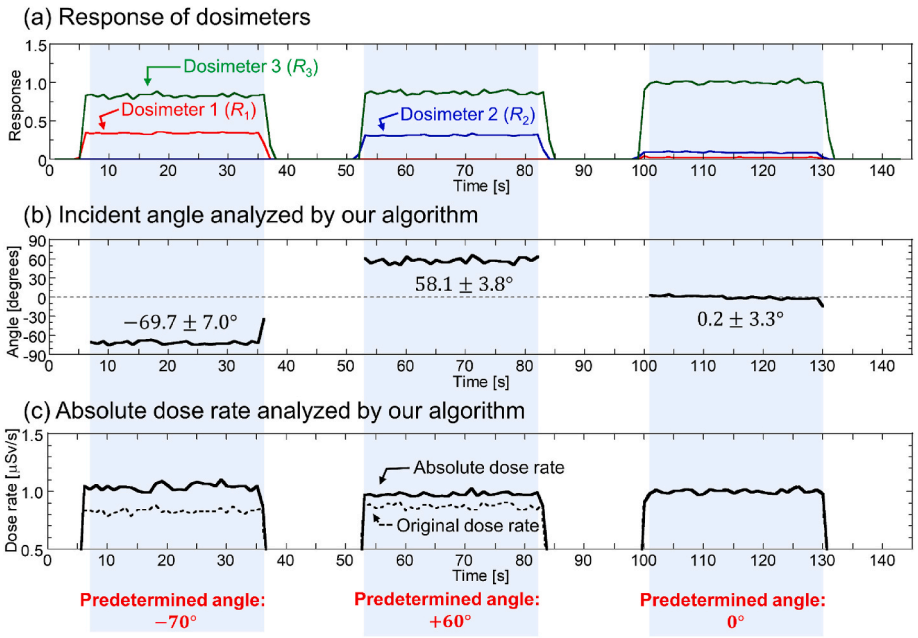

Fig. 6. Time-series measurement data to exemplify the availability of the modified triple-type dosimeter. Typical predetermined angles of −70°, +60°, and 0° are presented. Panel (a) shows responses from the dosimeters recorded at 1-s intervals. Panel (b) indicates the incident angles analyzed by our algorithm. Panel (c) shows a comparison between the original dose rate (without correction) and the absolute dose rate calculated using our algorithm with correction for the angular dependence.

related to the angular dependence. As shown in the right graph, although the mean original dose rate was 0.89 +/- 0.14 μSv/s (relative uncertainty of 15.2 %), the absolute dose rate was determined to be 1.00 +/- 0.03 μSv/s (relative uncertainty of 3.2 %).

4. Discussion

4.1. Improvement from the previous triple-type dosimeter

The concept of a triple-type dosimeter system (see Fig. 1), that can analyze both the incident angle of X-rays and the absolute dose by correcting for the angular dependence of active-type dosimeters, was proposed. Table 1 summarizes the specifications of this earlier version. Although previous studies have proposed the concept of a triple-type dosimeter, in those proposals the three dosimeters were arranged in a "straight line", which resulted in a narrow angular view of −50° to +50° [Asahara et al., 2023, 2024]. The present study aimed to expand the analytical field of angular view. The biggest change to the detection system was that the two dosimeters placed on the sides (dosimeter 1: left; dosimeter 2: right) were tilted at −45° and +45° and situated on the "arc" of a circle to accurately detect the angle of X-rays coming from the negative and positive directions. As shown in Fig. 4, each detector showed the expected angular dependence; dosimeter 1 achieved a measurable field of view of 0° to −80°, and dosimeter 2 achieved a measurable field of view of 0° to +80°. As a result, the improved triple-type dosimeter successfully achieved a field of view of −80° to +80°.

To account for the modified detector arrangement, the analysis algorithm was also modified. Fig. 8 shows the changes in the analysis algorithm from the previous studies. Fig. 8 (a) shows the incident angle calculation algorithm used in our previous papers [Asahara et al., 2023, 2024]. In this earlier algorithm, the vector R_{XY} was calculated from the signal difference between R_1 and R_2:

$$R_{XY} = \left\{ \frac{R_1}{\sqrt{{R_1}^2 + {R_2}^2}}, \frac{R_2}{\sqrt{{R_1}^2 + {R_2}^2}} \right\}. \quad (6)$$

This vector changes depending on θ_{in}. Reference data of R_{XY} were obtained in advance for predetermined angles (θ = −50°, …, −10°, 0°, +10°, …, +50°). The experimentally determined R_{XY} was plotted by the discrete "scatter plot" for comparison with the reference R_{XY}, and the X-ray incident angle was determined by adopting the θ_{in} associated with the closest reference R_{XY}. Although this algorithm required complex calculations, the accuracy of the calculated θ_{in} was very rough, as it was determined at 10° intervals. There was considered to be clear room for improvement in the algorithm used to calculate the incident direction of X-rays.

Our present procedure of the system is shown in Fig. 8 (b) (see also Fig. 2). Here, a simple algorithm is adopted that uses the signal difference between the detector located in the center and either the left or right detector, whichever has the larger signal. Since the function for calculating the X-ray incident angle is continuous, θ_{in} can be determined with high accuracy. In fact, in the experimental evaluation shown in Fig. 7, the incident angle was successfully calculated with an accuracy of ±1.35°. This is a significant technological advancement.

Improving the accuracy of θ_{in} can also improve the estimation accuracy of the correction coefficient (equation (4)) when calculating D_{abs}. As can be seen in Table 1, the uncertainty in the D_{abs} calculated using the previous algorithm was ±4.2 %, but that calculated using the revised algorithm was ±3.2 %, indicating an improvement in accuracy. As shown in Fig. 7, without the correction of the angular dependence, the systematic uncertainty increases to ±15.2 %, which is the biggest drawback of active-type dosimeters. Our present system could thus lift the main constraint to the clinical application of active-type dosimeters.

4.2. Clinical applicability and limitations

The triple-type dosimeter system demonstrated in this study can perform time-dependent analysis of both the incident angle and absolute dose. This capability would be useful for evaluating occupational exposure during IVR procedures. In recent years, the high dose level of occupational radiation exposure of medical staff during IVR procedures and orthopedic surgery [Yamashita et al., 2016, 2017; Nakajima et al.,

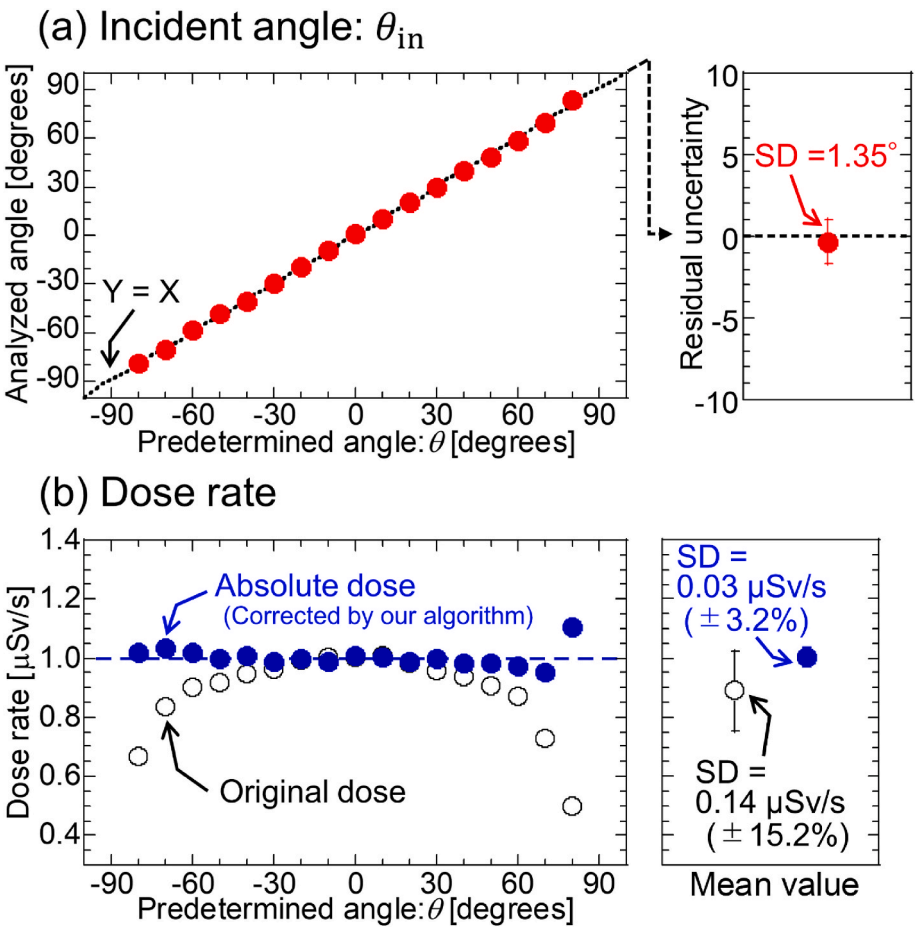

Fig. 7. Results of comparative experiments to verify the accuracy of the methodology for each X-ray incident angle. Panel (a) shows the results of the incident angle. θ_{in} could be analyzed in the angular view of −80° to +80° with an uncertainty of SD = ±1.35°. Panel (b) shows the dose rates determined from dosimeter 3. Absolute dose rates, which were corrected for angular dependence, did not include systematic uncertainty. The uncertainty of the dose rate was determined to be SD = ±0.03 μSv/s.

Table 1
A comparison of detector constructions between the previous studies and the present study.

	Previous study	Present study
References	Asahara et al. (2023) Asahara et al. (2024)	–
Dosimeter construction	Three **linearly arranged** detectors	Three detectors arranged on a **circular arc**[a]
Dosimeters used	RaySafe i2 (side × 2, center × 1)	RaySafe i2 × 2 (side × 2) RaySafe i3 × 1 (center × 1)[b]
Concept	(1) Incident angle determination (2) Absolute dose determination	(1) Incident angle determination (2) Absolute dose determination
Algorithm to derive the X-ray incident angle	Differences between side dosimeters	Differences between center and side dosimeters[b]
Applicable angular range	Angles: −50° to +50° at 10° intervals	Angles: −80° to +80°[c] (SD = ±1.35°)
Applicable photon energy	Scattered X-rays for 80 kV	Scattered X-rays for 80 kV
Systematic uncertainty of measured dose	±4.2 %	SD = ±3.2 %[c]

[a] The dosimeter design was reconsidered in this study.
[b] These contents were updated.
[c] See results in Fig. 7.

2025] has become a problem, and numerous studies on radiation protection have been conducted [Apostolou et al., 2025; Crowhurst et al., 2023; Hayashi et al., 2024]. It has been reported that the use of a shielding device can reduce radiation dose [Apostolou et al., 2025; Crowhurst et al., 2023], but it is difficult to confirm that the shielding device was functioning properly in these studies, since the incident direction of X-rays was not analyzed. By analyzing both the dose data and X-ray incident angle second-by-second, it becomes possible to more accurately assess the effectiveness of radiation protection and to investigate optimal radiation shielding procedures.

In clinical IVR procedure, the main cause of occupational exposure is scattered X-rays generated by the patient, and it is important to evaluate them. The proposed dosimeter was designed to estimate the incident angle in the horizontal (left-right) direction only. This is because the vertical location of the patient rarely changes during clinical IVR procedure. However, differences in the vertical scattered radiation distribution may occur depending on the height of the surgeon. If it becomes necessary in the future to determine the vertical incident angle, by

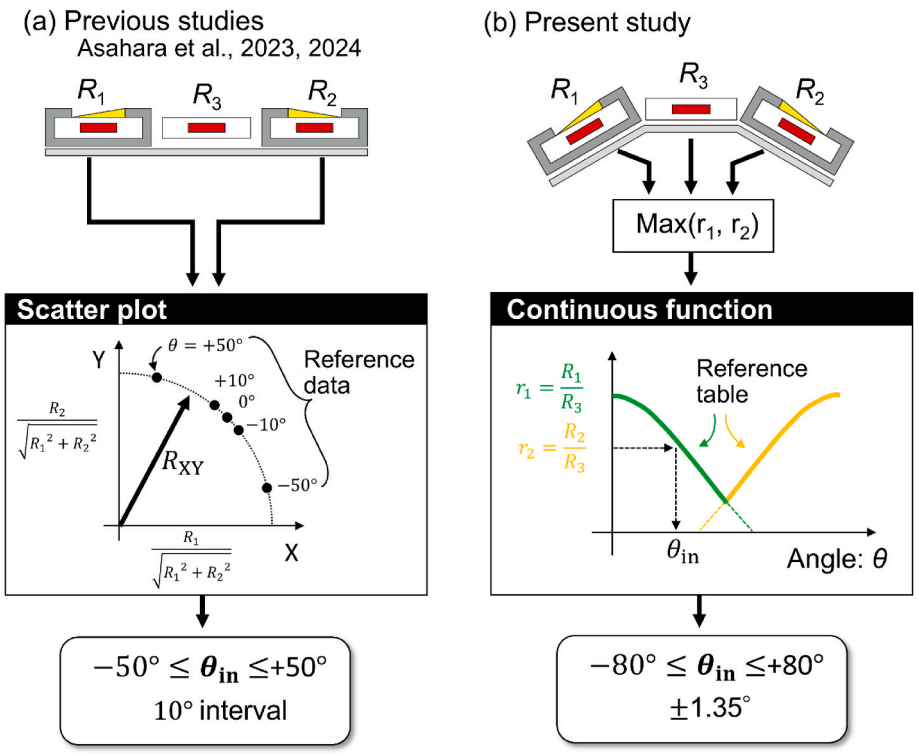

Fig. 8. Comparison of the detector construction and the analysis algorithm between the previous and present studies. In the previous method shown in (a), θ_{in} was calculated from the signal difference between the left and right detectors. θ_{in} could be calculated within the angular view of −50° to +50° at 10° intervals. In the detector shown in (b), the signal difference between the center detector and the left and/or right detectors is made based on a function of θ. Continuous analysis of θ_{in} can be performed within the view of −80° to +80° with an uncertainty of ±1.35°.

Table 2
Estimation of the lower deteion limit of our dosimeter.

Angle [degree]	Lower detection limit of dose rate [μSv/s]			
	Dosimeter 1[a] (RaySafe i2, left)	Dosimeter 2[a] (RaySafe i2, right)	Dosimeter 3[b] (RaySafe i3, center)	Estimated value for our system[c]
−80	0.035	–	0.013	0.035
−70	0.034	–	0.010	0.034
−60	0.034	–	0.010	0.034
−50	0.037	–	0.009	0.037
−40	0.042	–	0.009	0.042
−30	0.050	–	0.009	0.050
−20	0.070	–	0.008	0.070
−10	0.151	–	0.008	0.151
0	–	–	0.008	0.008
+10	–	0.087	0.008	0.087
+20	–	0.061	0.008	0.061
+30	–	0.048	0.009	0.048
+40	–	0.041	0.009	0.041
+50	–	0.037	0.009	0.037
+60	–	0.034	0.009	0.034
+70	–	0.034	0.011	0.034
+80	–	0.042	0.016	0.042

[a] The lower detectable limit of dosimeters 1 and 2 was reported to be 0.011 μSv/s, which is the minimum measurable dose rate for the RaySafe i2 dosimeter. These columns show the minimum detectable dose taking into account the attenuation of X-rays by the Ti slope filter.

[b] The lower detectable limit of dosimeter 3 was reported to be 0.008 μSv/s, which is the minimum measurable dose rate for the RaySafe i3. In this column, angular dependence was taken into consideraon.

[c] The detection limit for the entire system was estimated as the largest of the values in the first to third columns.

adding two detectors in the vertical position (up and down) in addition to the horizontal (left and right) detectors arrangement will achieve three-dimensional angle identification.

The lower detection limit (LDL) for our system was estimated as follows. The user manuals for the RaySafe i2 and RaySafe i3 dosimeters give lower detection limits of 0.011 μSv/s (=40 μSv/h) [Unfors RaySafe, 2014] and 0.008 μSv/s (=30 μSv/h) [Unfors RaySafe, 2020] for these devices, respectively. Because detectors 1 and 2 were fitted with Ti filters, the modified detection limits were calculated taking into account the attenuation in the filters, as shown in Table 2. On the other hand, for detector 3, only the angular dependence was accounted for when calculating the detection limit (see Fig. 4). The last column of Table 2 lists the larger value of the detection limits mentioned above, which is the detection limit for our system. Although the detection limit varies depending on the X-ray incident angle, it was shown that our dosimeter functioned correctly for doses above 0.151 μSv/s (=0.54 mSv/h). This detection limit is sufficient for clinical application. In previous studies, dose rates during IVR procedures have ranged from 0.054 to 16.4 mSv/h [Sanchez et al., 2010], 2–3 mSv/h [Vano et al., 2011], and 0.215–0.345 μSv/s under low-dose protocols [Zhang et al., 2021]. All of these reported values are above the LDL of our dosimeter, making the triple-type dosimeter applicable in a wide range of clinical IVR situations.

There are some limitations to this study. First, the purpose of this study was to demonstrate the feasibility of the proposed concept, and the experiments were performed at one specific measurement position. The reference tables and the correction factor used in the analysis algorithm were applied based on the calibration data acquired at this position. When performing actual measurements, the dosimeter may be worn at different heights or positions depending on the operator's physique. In such cases, the reference data calibrated at the corresponding

measurement position needs to be applied for the analysis. Therefore, further studies are needed to verify the accuracy of angle and dose analysis when the dosimeter is worn under different positional conditions. Second, the experiment was conducted using a simplified phantom and only 80 kV X-rays. Since the $r_1^{\mathrm{ref}}(\theta)$, $r_2^{\mathrm{ref}}(\theta)$, and k_θ, which are used as reference data for the algorithm, depend on the experimental conditions such as phantom size and tube voltage, the necessity of recalibration for each condition and/or further validation are required for application in actual clinical settings. Finally, while this study demonstrated the proof-of-concept, redesign is necessary for developing a compact product for this application.

5. Conclusion

A triple-type dosimeter system consisting of three active-type dosimeters was developed, enabling determination of both the incident angle and the absolute dose of X-rays. The two side detectors have slope filters in front of the window, and are placed on a circular arc. Experimental verification using a clinical fluoroscopy system was performed.

The incident angle was determined based on the signal difference between the side detector and a central detector. Based on experimental evaluation, it was found that our dosimeter system could determine the incident angle within an angular view of -80° to $+80^\circ$ with an uncertainty of $\pm 1.35^\circ$. The absolute dose was determined by eliminating the angular dependence using the determined incident angle. The systematic uncertainty in absolute dose rate was evaluated to be 3.2 %, versus 15.2 % when not applying angular dependence correction.

Our system is not only capable of calculating angle-corrected absolute dose values with high accuracy, but is also expected to enable research into further radiation exposure reduction using the information on the X-ray incident angle.

CRediT authorship contribution statement

Takashi Asahara: Writing – original draft, Investigation, Funding acquisition, Formal analysis, Data curation. **Rina Nishigami:** Writing – review & editing. **Daiki Kobayashi:** Software, Conceptualization. **Natsumi Kimoto:** Writing – review & editing, Conceptualization. **Sota Goto:** Writing – review & editing, Conceptualization. **Kazuki Takegami:** Writing – review & editing. **Rin Ishii:** Writing – review & editing. **Mana Mitani:** Writing – review & editing. **Mitsugi Honda:** Writing – review & editing, Data curation. **Toshihiro Iguchi:** Writing – review & editing, Supervision. **Hiroaki Hayashi:** Writing – original draft, Supervision, Funding acquisition, Conceptualization.

Funding source

This study was funded by Grants-in-Aid for Scientific Research [KAKENHI: 24K23055, 24K03306, 25K21600, 25K21586].

Declaration of competing interest

The authors declare the following financial interests/personal relationships which may be considered as potential competing interests: Takashi ASAHARA received research funding from JSPS KAKENHI grants (24K23055 & 25K21586), the Teraoka Scholarship Foundation (2024), the Cardiovascular Research Fund (2024), and the Kurata Grants from the Hitachi Global Foundation (2024). Daiki KOBAYASHI received a research funding from JSPS KAKENHI grant (25KJ1355). Natsumi KIMOTO received a research funding from JSPS KAKENHI grant (25K21600). Sota GOTO received a research funding from JSPS KAKENHI grant (24K21135). Hiroaki HAYASHI received a research funding from JSPS KAKENHI grant (JP24K03306).

Acknowledgement

The authors are very grateful to Mr. Takeshi Matsuoka, Mr. Shigenori Sakurai and Mr. Hioroshi Saito at the Kanazawa University Technical Support Center for helping us to fabricate the experimental apparatuses. This study was conducted using the clinical fluoroscopic equipment at Okayama University Hospital, Japan. We would like to thank the medical staff who manage the equipment.

Data availability

Data will be made available on request.

References

Apostolou, A., Leichert, H.J., König, A.M., Owczarek, A.D., Mahnken, A.H., 2025. Efficiency in radiation protection of a novel exoskeleton-based interventional radiology apron and correlation with conventional aprons. Eur. J. Radiol. 184, 111946. https://doi.org/10.1016/j.ejrad.2025.111946.

Asahara, T., Hayashi, H., Goto, S., Tomita, E., Kimoto, N., Mihara, Y., Asakawa, T., Kanazawa, Y., Katsumata, A., Higashino, K., Yamashita, K., Okazaki, T., Hashizume, T., 2018. Exposure dose measurement during diagnostic pediatric X-ray examination using an optically stimulated luminescence (OSL) dosimeter based on precise dose calibration taking into consideration variation of X-ray spectra. Radiat. Meas. 119, 209–219. https://doi.org/10.1016/j.radmeas.2018.10.007.

Asahara, T., Hayashi, H., Goto, S., Kimoto, N., Takegami, K., Maeda, T., Kanazawa, Y., Okazaki, T., Hashizume, T., 2020. Evaluation of calibration factor of OSLD toward eye lens exposure dose measurement of medical staff during IVR. J. Appl. Clin. Med. Phys. 21, 263–271. https://doi.org/10.1002/acm2.13042.

Asahara, T., Hayashi, H., Maeda, T., Goto, S., Kobayashi, D., Nishigami, R., Lee, C., Ando, M., Kanazawa, Y., Imajo, S., Yamashita, K., Higashino, K., 2023. A wearable active-type X-ray dosimeter having novel functions to derive both incident direction and absolute exposure dose. Radiat. Phys. Chem. 208, 110932. https://doi.org/10.1016/j.radphyschem.2023.110932.

Asahara, T., Hayashi, H., Maeda, T., Kobayashi, D., Nishigami, R., Goto, S., Ando, M., Kimoto, N., Kanazawa, Y., Yamashita, K., 2024. Evaluation of lower detection limit and performance analyses related to the incident angle of X-rays and absolute dose using a triple-type dosimeter. Radiat. Meas. 175, 107148. https://doi.org/10.1016/j.radmeas.2024.107148.

Cardoso, J., Santos, J.A., Santos, L., Alves, J.G., Oliveira, C., 2016. Characterization of an active dosemeter according to iec 61526:2010. Radiat. Protect. Dosim. 170, 127–131. https://doi.org/10.1093/rpd/ncw090.

Cewe, P., Vorbau, R., Omar, A., Elmi-Terander, A., Edström, E., 2022. Radiation distribution in a hybrid operating room, utilizing different X-ray imaging systems: investigations to minimize occupational exposure. J. Neurointerventional Surg. 14, 1139–1144. https://doi.org/10.1136/neurintsurg-2021-018220.

Crowhurst, J.A., Tse, J., Mirjalili, N., Savage, M.L., Raffel, O.C., Gaikwad, N., Walters, D. L., Dautov, R., 2023. Trial of a novel radiation shielding device to protect staff in the cardiac catheter laboratory. Am. J. Cardiol. 203, 429–435. https://doi.org/10.1016/j.amjcard.2023.07.050.

Dong, K.R., Kweon, D.C., Chung, W.K., Goo, E.H., Dieter, K., Choe, C.H., 2011. Study on the angular dependence of personal exposure dosimeter - focus on thermoluminescent dosimeter and photoluminescent dosimeter. Ann. Nucl. Energy 38, 383–388. https://doi.org/10.1016/j.anucene.2010.10.003.

Gangl, A., Deutschmann, H.A., Portugaller, R.H., Stücklschweiger, G., 2022. Influence of safety glasses, body height and magnification on the occupational eye lens dose during pelvic vascular interventions: a phantom study. Eur. Radiol. 32, 1688–1696. https://doi.org/10.1007/s00330-021-08231-y.

Goto, S., Hayashi, H., Asahara, T., Kimoto, N., Tomita, E., Takegami, K., Asakawa, T., Kanazawa, Y., Okazaki, T., Hashizume, T., 2020. An idea to reduce angular dependence of dosimeter having a disk-shaped detection region. Radiat. Meas. 137, 106323. https://doi.org/10.1016/j.radmeas.2020.106323.

Goto, S., Hayashi, H., Yamaguchi, H., Sekiguchi, H., Akino, R., Shimizu, M., 2023. Signal-stabilized Al_2O_3:C-OSL dosimeter "checking chip" for correcting OSL reader sensitivity variation. Radiat. Meas. 160, 106893. https://doi.org/10.1016/j.radmeas.2022.106893.

Goto, S., Maeda, T., Takegami, K., Nishigami, R., Kobayashi, D., Asahara, T., Kimoto, N., Kanazawa, Y., Yamashita, K., Higashino, K., Konishi, T., Maki, M., Hayashi, H., 2025. A novel analytic procedure for accurate patient surface dose measurement during computed tomography examination: systematic uncertainty correction related to incident X-ray direction. Radiat. Phys. Chem. 230, 112551. https://doi.org/10.1016/j.radphyschem.2025.112551.

Hattori, K., Inaba, Y., Kato, T., Fujisawa, M., Yasuno, H., Yamada, A., Haga, Y., Suzuki, M., Zuguchi, M., Chida, K., 2023. Evaluation of a new real-time dosimeter sensor for interventional radiology staff. Sensors 23, 512. https://doi.org/10.3390/s23010512.

Hayashi, H., Kimoto, N., Maeda, T., Tomita, E., Asahara, T., Goto, S., Kanazawa, Y., Shitakubo, Y., Sakuragawa, K., Ikushima, H., Okazaki, T., Hashizume, T., 2021. A disposable OSL dosimeter for in vivo measurement of rectum dose during brachytherapy. Med. Phys. 48, 4621–4635. https://doi.org/10.1002/mp.14857.

Hayashi, H., Maeda, T., Takegami, K., Nishigami, R., Kobayashi, D., Asahara, T., Goto, S., Kimoto, N., Kanazawa, Y., Yamashita, K., Higashino, K., Murakami, S., Konishi, T.,

Maki, M., 2024. A suitable procedure of dose reduction factor measurements of X-ray shields during computed tomography examination - the importance of considering positional changes of an X-ray tube. Radiat. Phys. Chem. 222, 111880. https://doi.org/10.1016/j.radphyschem.2024.111880.

Hayashi, H., Maeda, T., Takegami, K., Goto, S., Asahara, T., Kimoto, N., Nishigami, R., Kobayashi, D., Kanazawa, Y., Yamashita, K., Konishi, T., Maki, M., 2025. Impact of different X-ray tube positions on actual dose measurements during CT examinations -An effect of patient physique-. Radiat. Phys. Chem. 237, 113001. https://doi.org/10.1016/j.radphyschem.2025.113001.

Hayasahi, H., Takegami, K., Nishigami, R., Kobayashi, D., Goto, S., Asahara, T., Kimoto, N., Takemitsu, M., Ishii, R., Morimoto, S., Maki, M., 2026. Experimental approach of internal dose map visualization during helical CT examinations: importance of X-ray incident direction analysis and central internal dose estimation. Radiat. Meas. 191, 107586. https://doi.org/10.1016/j.radmeas.2025.107586.

Japan Industrial Standard (JIS) Z4915: 1974, 1974. X-ray Water Phantom for Chest and Abdomen. Japanese Standards Association, Tokyo, Japan.

Jursinic, P.A., 2007. Characterization of optically stimulated luminescent dosimeters, OSLDs, for clinical dosimetric measurements. Med. Phys. 34, 4594–4604. https://doi.org/10.1118/1.2804555.

Lundvall, L.L., Sandborg, M., 2022. Does radiological protection training or a real-time staff dosemeter display reduce staff doses during X-RAY-GUIDED pulmonary bronchoscopy? Radiat. Protect. Dosim. 198, 265–273. https://doi.org/10.1093/rpd/ncac028. PMID: 35348761; PMCID: PMC9040482.

Maeda, T., Takegami, K., Goto, S., Asahara, T., Kobayashi, D., Nishigami, R., Kimoto, N., Yamashita, K., Higashino, K., Morimoto, S., Konishi, T., Maki, M., Hayashi, H., 2026. Helical X-ray Tube Trajectory Estimation via Image Noise Analysis for Enhanced CT Dosimetry. Radiat. Phys. Chem. 239, 113260. https://doi.org/10.1016/j.radphyschem.2025.113260.

Mangiarotti, M., D'Ercole, L., Quaretti, P., Moramarco, L., Lafe, E., Zappoli Thyrion, F., 2016. Evaluation of an active personal dosimetry system in interventional radiology and neuroradiology: preliminary results. Radiat. Protect. Dosim. 172, 483–487. https://doi.org/10.1093/rpd/ncv502, 2016.

Nakajima, D., Yamashita, K., Omichi, Y., Tamaki, Y., Hayashi, H., Higashino, K., Tsuruo, Y., Sairyo, K., 2025. Occupational radiation exposure for a spinal interventionalist performing fluoroscopic selective nerve root block: a cadaveric study. Spine Surg. Relat. Res. 2025-0064 (2025DOI). https://doi.org/10.22603/ssrr.2025-0064.

Sanchez, R., Vano, E., Fernandez, J.M., Gallego, J.J., 2010. Staff radiation doses in a real-time display inside the angiography room. Cardiovasc. Interv. Radiol. 33, 1210–1214. https://doi.org/10.1007/s00270-010-9945-4.

Sanchez, R.M., Vano, E., Salinas, P., Gonzalo, N., Escaned, J., Fernández, J.M., 2021. High filtration in interventional practices reduces patient radiation doses but not always scatter radiation doses. Br. J. Radiol. 94, 20200774. https://doi.org/10.1259/bjr.20200774.

Silva, E.H., Knežević, Ž., Struelens, L., Covens, P., Ueno, S., Vanhavere, F., Buls, N., 2016. Energy and angular dependence of radiophotoluminescent glass dosemeters for eye lens dosimetry. Radiat. Protect. Dosim. 170, 208–212. https://doi.org/10.1093/rpd/ncw104.

Takegami, T., Hayashi, H., Maeda, T., Lee, C., Nishigami, R., Asahara, T., Goto, S., Kobayashi, D., Ando, M., Kanazawa, Y., Yamashita, K., Higashino, K., Murakami, S., Konishi, T., Maki, M., 2023. Thyroid dose reduction shield with the generation of less artifacts used for fast chest CT examination. Radiat. Phys. Chem. 203, 110635. https://doi.org/10.1016/j.radphyschem.2022.110635.

Unfors RaySafe, 2014. RaySafe i2 user manual. https://www.raysafe.com/sites/default/files/2018-12/5001050-raysafe-i2-service_manual-en-c.pdf.

Unfors RaySafe, 2020. RaySafe i3 user manual. https://www.raysafe.com/sites/default/files/6012549f_en_RaySafe_i3_Brochure.pdf.

Vano, E., Fernandez, J.M., Sanchez, R., 2011. Occupational dosimetry in real time. Benefits for interventional radiology. Radiat. Meas. 46, 1262–1265. https://doi.org/10.1016/j.radmeas.2011.04.030.

Yamashita, K., Higashino, K., Wada, K., Morimoto, M., Abe, M., Takata, Y., Sakai, T., Fukui, Y., Sairyo, K., 2016. Radiation exposure to the surgeon and patient during a fluoroscopic procedure: how high is the exposure dose? A cadaveric study. Spine 41, 1254–1260. https://doi.org/10.1097/BRS.0000000000001542.

Yamashita, K., Higashino, K., Hayashi, H., Hayashi, F., Fukui, Y., Sairyo, K., 2017. Pulsation and collimation during fluoroscopy to decrease radiation: a cadaver study. JB JS Open Access 19, e0039. https://doi.org/10.2106/JBJS.OA.17.00039.

Zhang, Z., Phang, C.C., Tan, R.Y., Pang, S.C., Chandramohan, S., Zhuang, K.D., Sulaiman, M.S., Tay, K.H., Chong, T.T., Tan, C.S., 2021. Does reducing radiation levels for procedures affect image quality and radiation to proceduralists? A double-blinded randomised study of two protocols. Clin. Radiol. 76, 157.e1–157.e10. https://doi.org/10.1016/j.crad.2020.09.003.